

**1 High-Resolution Late 21st-Century Projections of
2 Regional Precipitation by Empirical Downscaling
3 from Circulation Fields of the IPCC AR4 GCMs**

R. E. Nicholas^{1,2} and D. S. Battisti¹

David S. Battisti, Department of Atmospheric Sciences, University of Washington, Box 351640,
Seattle, WA 98195-1640 USA (battisti@u.washington.edu)

Robert E. Nicholas, Department of Geosciences, Pennsylvania State University, University
Park, PA 16802 USA (rob.nicholas@psu.edu)

¹Department of Atmospheric Sciences,
University of Washington, Seattle,
Washington, USA.

²Current address: Department of
Geosciences, Pennsylvania State University,
University Park, Pennsylvania, USA.

4 In a previous study, the authors described a methodology for statistical/empirical
5 downscaling from low-resolution circulation fields to high-resolution regional
6 precipitation. Empirical downscaling models (EDMs) were constructed us-
7 ing the relationship between variability in large-scale reanalysis predictor fields
8 and observed monthly mean precipitation over four regions: the Southeast
9 United States, the Upper Colorado River basin, China's Jiangxi Province,
10 and a portion of Central Europe. Here, these models are applied to predic-
11 tor fields obtained from global climate models (GCMs) participating in the
12 Coupled Model Intercomparison Project Phase 3 (CMIP3) to obtain alter-
13 nate projections of precipitation changes between the late 20th and late 21st
14 centuries. For three of the four regions, the annual cycle of precipitation for
15 the late 20th century obtained from the ensemble average of the CMIP3 mod-
16 els using EDMs more closely matches observed precipitation than that ob-
17 tained directly from the GCMs and for all regions the intermodel spread in
18 the empirically downscaled climatology is substantially reduced. This supports
19 the hypothesis that regional precipitation is primarily determined by large-
20 scale circulation fields and that the latter are well-represented across the CMIP3
21 models. The EDMs are then used to calculate projected changes in the an-
22 nual cycle of precipitation for the late 21st century due to global warming.
23 Although the projected changes (1950-1999 to 2050-2099) are modest for both
24 the raw and downscaled model results, the downscaled product shows much
25 greater agreement across models, suggesting a greater confidence in projected

26 precipitation changes can be obtained efficiently using empirical downscal-
27 ing.

1. Introduction

28 From the perspective of planning and adaptation, precipitation is one of the primary
29 variables of interest in studies of potential changes in the climate system due to anthro-
30 pogenic greenhouse warming because of its importance for water supply, agriculture, flood
31 control, and ecosystems. Climatological precipitation varies on small spatial scales, es-
32 pecially in the presence of complex topography, that cannot be resolved by the present
33 generation of global climate models (GCMs) such as those participating in the 3rd Cou-
34 pled Model Intercomparison Project. Furthermore, these models display large biases in
35 precipitation over many regions and the spread in projected future changes is often much
36 larger than the ensemble mean change. As a way of circumventing these deficiencies,
37 both dynamical and empirical/statistical downscaling approaches have been employed to
38 generate precipitation projections at higher spatial resolution. Each of these approaches
39 comes with a variety of advantages and disadvantages, which are discussed at length by
40 *Benestad et al.* [2008] and *Nicholas and Battisti* [2011]. Perhaps the most compelling
41 advantage of the empirical/statistical approach is computational efficiency, which makes
42 the generation of large ensembles of projections a much more tractable proposition than
43 it would be using a regional climate model (RCM).

44 In this study, the empirical/statistical downscaling approach described by *Nicholas and*
45 *Battisti* [2011], and similar to that previously employed by *Widmann et al.* [2003] and
46 *Vimont et al.* [2009], is applied to large-scale predictor fields obtained from the CMIP3
47 archive to produce ensemble projections of changes in the annual cycle of monthly mean
48 precipitation between 1950-1999 and 2050-2099 as described in section 2. In section 3 we

49 show the results of ensemble projections for four regions — the U.S. Southeast, the Upper
50 Colorado River basin, China’s Jiangxi Province, and Central Europe – and compare these
51 with projected changes in precipitation from the GCMs themselves. Section 4 offers some
52 concluding remarks on utility and implications of such projections.

2. Data and methods

53 *Nicholas and Battisti* [2011] describe a method for empirical downscaling of monthly-
54 mean precipitation from large-scale predictor fields obtained from reanalysis. Briefly, the
55 empirical downscaling model (EDM) is “trained” by regressing observed (in this case, high-
56 resolution gridded) precipitation onto time variations in the leading patterns of large-scale
57 predictor fields. By projecting the identified patterns onto an independent set of large-
58 scale predictor fields and applying the associated regressions to the resulting timeseries,
59 predictions of precipitation may be obtained at the resolution of the observed precipi-
60 tation. Although a variety of methods can be used to identify the relevant patterns of
61 large-scale variability, *Nicholas and Battisti* [2011] found that using standard empirical or-
62 thogonal function (EOF) analysis of predictor field combinations produced skillful results
63 (in terms of replicating both the annual cycle and monthly anomalies) in cross-validation
64 tests, often exceeding the skill of precipitation derived directly from reanalysis.

65 In this study, we apply the same method, generating EDMs of precipitation using
66 monthly-mean predictor fields obtained from the NCEP-NCAR Reanalysis project (NNR
67 [*Kalnay et al.*, 1996]) and 0.5° gridded precipitation from the University of Delaware Ter-
68 restrial Precipitation dataset version 2.01 (UDel) for the period 1949-2008. The skill of
69 the EDM is determined using cross-validation and the metrics described in *Nicholas and*

70 *Battisti* [2011], and is discussed briefly below. Next, hindcasts of 1950-1999 precipita-
 71 tion are generated by applying the EDMs to predictor fields obtained from 20th century
 72 commitment scenario (20c3m) runs of 18 models from the CMIP3 archive. Long-term
 73 monthly means are then calculated from each 600-month hindcast to obtain the annual
 74 cycle of precipitation for the period 1950-1999. The process is then repeated using out-
 75 put fields from A2 scenario (sresa2) runs of the same GCMs for the period 2050-2099
 76 to obtain projections of the annual cycle of regional-scale precipitation during the latter
 77 half of the 21st century. In instances where a model had multiple runs available for a
 78 given scenario, EDM projections for all runs were averaged to produce a single estimate
 79 of the annual cycle of precipitation for that model and scenario. The GCM predictor fields
 80 were interpolated to same 2.5° grid as the NNR predictor fields prior to downscaling. For
 81 comparison with observations and EDM results, GCM precipitation is interpolated to the
 82 same 0.5° grid as UDel. In section 3, we show these hindcasts, along with projections of
 83 expected changes in the annual cycle of precipitation, for each model and each region for
 84 selected predictor-variable combinations.

Since this study is only concerned with the annual cycle of precipitation (and changes in it), standard forecast assessment metrics are unhelpful for quantifying the skill of our EDMs. In lieu of such measures, we use the “annual cycle skill score” (ACSS) introduced by *Nicholas and Battisti* [2011]:

$$\text{ACSS} = 1 - \sqrt{\frac{\sum_{i,j,k} [\cos \theta_j \cdot (\hat{f}_{ijk} - \hat{x}_{ijk})^2]}{\sum_{i,j,k} [\cos \theta_j \cdot \hat{x}_{ijk}^2]}}$$

85 Here, the indices i , j , and k denote (respectively) times, latitude, and longitude in the
 86 forecast domain; \hat{f}_{ijk} is the forecast/hindcast local climatological mean precipitation for

87 a given calendar month, \hat{x}_{ijk} is the observed local climatological mean precipitation for a
 88 given month, and θ_j is the latitude for each location. This measure is similar to the RMS
 89 skill score (RMSSS [WMO, 2002]) except that it is weighted by the sum of the squares of
 90 the climatological mean for each month and location. Thus, a given absolute error carries
 91 a smaller penalty when true climatological monthly mean at that location is large. The
 92 cosine term provides area weighting for each gridbox, although the domains used in this
 93 study are sufficiently small that the inclusion of this term has little effect on the result.
 94 The maximum value for ACSS is 1 for a “perfect” hindcast; ACSS may be negative and
 95 there is no lower bound.

96 This procedure was used to downscale precipitation over four regions: interior Southeast
 97 United States, the Upper Colorado River Basin in western Colorado and eastern Utah,
 98 Jiangxi Province in southeastern China, and a portion of Central Europe including the
 99 Czech Republic and parts of Germany, Poland, Austria, and Slovenia. To simplify the
 100 analysis, only one predictor variable set is examined for each region; the predictor chosen
 101 for each region was selected from among those described in *Nicholas and Battisti* [2011]
 102 such that high levels of skill in replicating both monthly anomalies and the annual cycle
 103 were achieved in cross-validation tests. Table 1 lists the predictor field sets, predictor
 104 domains, and test domains for each downscaling region.

Ensemble convergence is quantified using a spread score, S , defined as the mean absolute deviation from the ensemble mean projection for a particular month, averaged over all months:

$$S = \frac{1}{12M} \sum_{i,m}^M |P_{m,i} - \bar{P}_i|$$

105 Here, $P_{m,i}$ is climatological projection for a particular model, m , and month, i ; \bar{P}_i is the
106 ensemble mean climatological projection for a given month; and M is the total number of
107 ensemble members ($M = 18$ in the case of this study). Spread scores for all four regions
108 are shown in Table 2.

3. Results

3.1. Southeast United States

109 Results for precipitation downscaling over the interior Southeast United States are
110 shown in Figure 1. The predictor used is a combination of specific humidity, zonal wind,
111 and meridional wind at 850 mb (Q850-U850-V850) and is interpreted as a measure of
112 low-level moisture flux into the region. The top panel of Figure 1 shows the annual cycle
113 precipitation produced by all 18 GCMs examined in this study (blue) and statistically
114 downscaled using predictor fields from these same GCMs (red) for the period 1950-1999.
115 In general the GCMs tend to underestimate precipitation throughout most of the year,
116 with only two models showing the type of large summertime biases that *Nicholas and*
117 *Battisti* [2011] found in NNR. The EDM results tend to hew more closely to the observed
118 annual cycle from the GCMs (black), with an average ACSS of 0.795 compared with 0.683
119 for the GCMs. The middle panel shows projected 1950-1999 to 2050-2099 changes in the
120 annual cycle of precipitation for the 9 most skillful GCMs and EDMs; the bottom panel
121 shows these same changes represented as percentages of the observed monthly means for
122 the period 1950-1999. Although the ensemble mean of the projected changes is similar
123 for GCMs and EDMs, and generally small, there is considerably more spread in the direct

124 GCM projections, with some models showing decreases of up to 40% in certain months
125 (see Table 2 and Figure 1).

3.2. Upper Colorado River Basin

126 Results for precipitation downscaling over the Upper Colorado River Basin are shown
127 in Figure 2. The predictor used is a combination of specific humidity, temperature, and
128 meridional wind at 700 mb (Q700-T700-V700). GCMs consistently overpredict precip-
129 itation in most months of the year for this region, with excesses typically in the range
130 of 50-200%. The EDMs follow the observed annual cycle much more closely, albeit with
131 notable deficits in the summer months, and show considerably less spread than the GCMs
132 (Table 2 and top panel of Figure 2). The average ACSS for EDMs is 0.549 compared
133 with -0.131 for the GCMs. Projected 1950-1999 to 2050-2099 changes for the 9 most
134 skillful GCMs and EDMs (middle and bottom panels of Figure 2) have similar shapes,
135 with EDM ensemble mean showing a smaller springtime reduction and a larger increase in
136 the late summer through fall. The ensemble mean changes reach values of $\pm 30\%$ in some
137 months and could have a serious impact on water resources for this region; however, both
138 GCMs and (especially) EDMs show relatively small changes during the winter months,
139 when snowpack is produced.

3.3. Jiangxi Province, China

140 Jiangxi Province, comprised primarily of the Gan River basin, lies just south of the
141 Yangtze River and has a climate that is heavily influenced by the East Asian Monsoon.
142 The most prominent feature in annual cycle of precipitation, a gradual springtime rise
143 followed by a sharp drop in the early summer, is associated with the build-up and passage

144 of the Meiyu frontal zone. Downscaling results for this region are shown in Figure 3.
145 The predictor used is a combination of specific humidity at 850 mb and zonal winds
146 at both 850 and 300 mb. EDMs and GCMs perform similarly representing the annual
147 cycle of precipitation (top panel), with an average ACSS of 0.604 for EDMs compared
148 with 0.605 for GCMs; both generally fail to fully capture the sharp drop in precipitation
149 associated with the Meiyu passage. In the bottom two panels, notable differences between
150 the 1950-1999 to 2050-2099 changes for GCMs and EDMs are seen; while the GCM-
151 projected changes are relatively modest, with small reductions in fall/winter and modest
152 summertime increases, the EDMs show increases in all months, ranging from 10% in April
153 to as high as 50% in October. Jiangxi Province is already one of the wettest parts of China
154 and precipitation increases of the magnitude suggested by these EDMs, should they come
155 to pass, could have a serious impact on flooding in the region.

156 To further explore possible future changes in the East Asian Monsoon System, the same
157 EDM (that is, trained on Q850-U300-U850 over the same predictor domain) was used to
158 generate 1950-1999 hindcasts and 2050-2099 forecasts of land surface precipitation over
159 eastern China from the southern coast north to the Mongolian border (110° - 120° E, 21° -
160 42° N). In the top row of Figure 4, the zonal mean annual cycles of precipitation over the
161 region from ensemble mean GCM and EDM hindcasts are compared with the observed
162 annual cycle. Here, the EDMs clearly do a better job of replicating both the “shape” and
163 local magnitude of precipitation over the monsoon region although, as noted before, both
164 GCMs and EDMs fail to fully capture the sharp June-July drop in precipitation associated
165 with the northward passage of the Meiyu frontal zone out of Jiangxi. In the bottom row

166 of Figure 4, projected 1950-1999 to 2050-2099 changes from the 9 most skillful GCMs and
167 EDMs are shown in a similar calendar month versus latitude (Hovmoller) format. The
168 differences between the two sets of projections are striking. GCMs (Figure 4d), on average,
169 project small decreases in the the southern part of the domain throughout most of the
170 year, except for JJA, which corresponds with the peak of the GCMs' "monsoon." In the
171 northern part of the domain, increases are seen throughout the year, with larger increases
172 in mid-summer (suggesting a strengthened Meiyu) and early spring. By contrast, the
173 EDMs project increases in all parts of the domain in all seasons, with the largest absolute
174 increases (Figure 4e) roughly corresponding to the locations and times of highest peak
175 hindcast precipitation. In the already quite wet southern part of the domain, EDMs
176 project rain rates to increase by as much as 4 mm/day. However, relative to 1950-1999
177 observations, the EDM-projected changes (Figure 4f) look rather different, with the largest
178 percent changes seen during the winter in both the far southern and far northern parts of
179 the domain, where precipitation increases may reach 50%. That both GCMs and EDMs
180 project increasing precipitation (albeit with somewhat different seasonality) in water-
181 stressed but agriculturally important northern China is a particularly interesting result
182 given the much-discussed drying trend observed in this region.

3.4. Central Europe

183 The final region over which downscaling was performed is a portion of Central Europe,
184 that was examined by *Nicholas and Battisti* [2011] because NNR shows a large drop in
185 precipitation over this region around 1990 that does not appear in observations (nor does
186 it correspond to any similarly-timed jumps in precipitation over other regions). Downscal-

187 ing was performed using a combination of specific humidity and geopotential height at 850
188 mb (Q850-Z850) as the predictor; results are shown and compared with GCMs in Figure
189 5. GCMs tend to overestimate precipitation in this region, especially during the summer
190 months (also seen by *Nicholas and Battisti* [2011] in NNR precipitation), while EDMs
191 tend to overestimate precipitation from late fall through early spring (top panel). En-
192 semble mean ACSS for EDMs is 0.732 compared with 0.545 the corresponding 18 GCMs.
193 Projections from the 9 most-skillful GCMs show increases in the neighborhood of 10%
194 during fall, winter, and spring, with reductions of a similar magnitude during the summer
195 (bottom two panels); the spread in GCM-projected changes is particularly large for the
196 summer months, indicating a high level of uncertainty during this season. By contrast,
197 EDM-projected changes show increases equal to or exceeding those of the GCMs in all
198 months and with considerably less spread. EDM-projected changes are largest in spring
199 and smallest in summer, although these differences are relatively minor.

4. Discussion

200 Following on the work of *Nicholas and Battisti* [2011], this study uses the same empiri-
201 cal/statistical downscaling approach to project changes in precipitation between the late
202 20th and late 21st centuries. To do this, EDMs are first trained on reanalysis predictor
203 fields and observed precipitation, and then projections are made by applying the EDMs
204 to predictor fields obtained from models participating in CMIP3. For late 21st century
205 projections, we use model runs forced by the IPCC SRES A2 emissions scenario. The
206 EDM-generated precipitation is compared with precipitation obtained directly from the
207 GCMs themselves both in terms of skill and projected changes in the annual cycle.

208 The empirical models described here offer a plausible alternative to both global and
209 regional climate models for projections of future precipitation under climate change sce-
210 narios. In general, these EDMs achieve higher levels of skill in replicating the annual cycle
211 for precipitation during the observational period (1950-1999) than do the GCMs alone (for
212 Jiangxi Province, the EDM skill was slightly but not substantially, lower). For three of
213 the four regions investigated in this study, we found non-trivial differences between GCM
214 projections of late 21st century precipitation and the projections of EDMs “forced” by
215 circulation fields from these same GCMs. In general, the EDMs tend to project smaller
216 decreases and larger increases in precipitation compared to the corresponding GCMs, per-
217 haps because the EDMs are explicitly (and linearly) sensitive to increasing atmospheric
218 moisture content, whereas the impact of greater moisture availability is conditioned by
219 other processes in the GCMs. We note, however, that the ensemble spread in EDM pro-
220 jections is always smaller than for the corresponding GCM projections, indicating that
221 regional precipitation is primarily controlled by large scale circulation and that, across the
222 CMIP3 ensemble, the GCM-simulation circulation fields are quite similar to the observed
223 fields. These results suggest, somewhat surprisingly, that the potential reliability of fu-
224 ture projections of regional precipitation may be much greater than currently thought.
225 As such, empirical downscaling efforts similar to the one we have described here should
226 be considered, either alongside or perhaps even in place of dynamical models, in climate
227 impacts studies where precipitation (especially on monthly or seasonal mean timescales)
228 is the primary variable of interest.

229 **Acknowledgments.** The authors wish to thank the National Science Foundation
230 (grant number BCS-0624359) and the Tamaki Foundation for their support of this work.

References

- 231 Benestad, R. E., I. Hanssen-Bauer, and D. Chen (2008), Empirical-statistical downscaling,
232 p. 215 pp.
- 233 Kalnay, E., et al. (1996), The NCEP/NCAR 40-year reanalysis project, *Bulletin of the*
234 *American Meteorological Society*, 77(3), 437–471.
- 235 Nicholas, R. E., and D. S. Battisti (2011), Empirical downscaling of high-resolution re-
236 gional precipitation from large-scale reanalysis fields, *Journal of Applied Meteorology*
237 *and Climatology*, in press.
- 238 Vimont, D. J., D. S. Battisti, and R. L. Naylor (2009), Downscaling Indonesian pre-
239 cipitation using large-scale meteorological fields, *International Journal of Climatology*,
240 published online 24 August 2009.
- 241 Widmann, M., C. Bretherton, and E. Salathé (2003), Statistical precipitation downscaling
242 over the northwestern United States using numerically simulated precipitation as a
243 predictor, *Journal of Climate*, 16(5), 799–816.
- 244 WMO (2002), Standardised verification system (SVS) for long-range forecasts (LRF),
245 *Tech. rep.*, World Meteorological Organization, attachment II-9 to the Manual on the
246 GDPS (WMO 485), Vol. I.

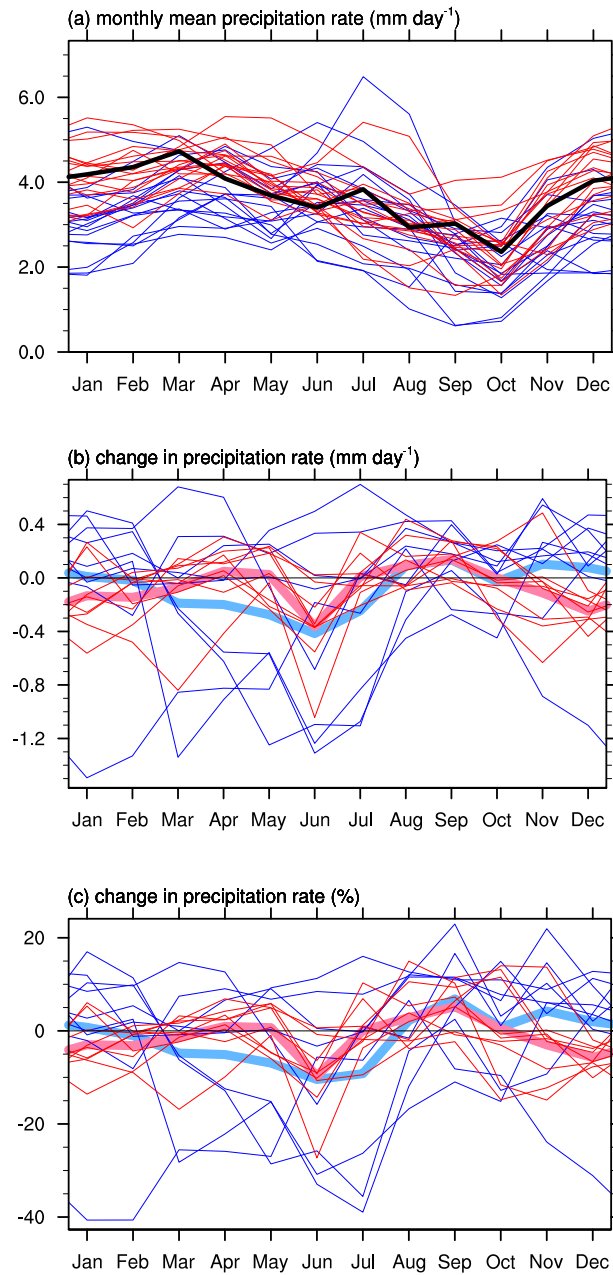


Figure 1. (a) Annual cycle of precipitation from observations (black), 18 AR4 GCMs (thin blue), and EDMs driven by Q850-U850-V850 predictor fields from these 18 GCMs (thin red) over the Southeast US for the period 1950-1999. Projected 1950-1999 to 2050-2099 changes in precipitation for the 9 most skillful GCM and EDM hindcasts are shown (b) in mm/day and (c) as a percentage of the observed monthly mean for the period 1950-1999. Broad colored lines indicate ensemble means. Ensemble mean ACSS is 0.82 for EDMs and 0.73 for GCMs.

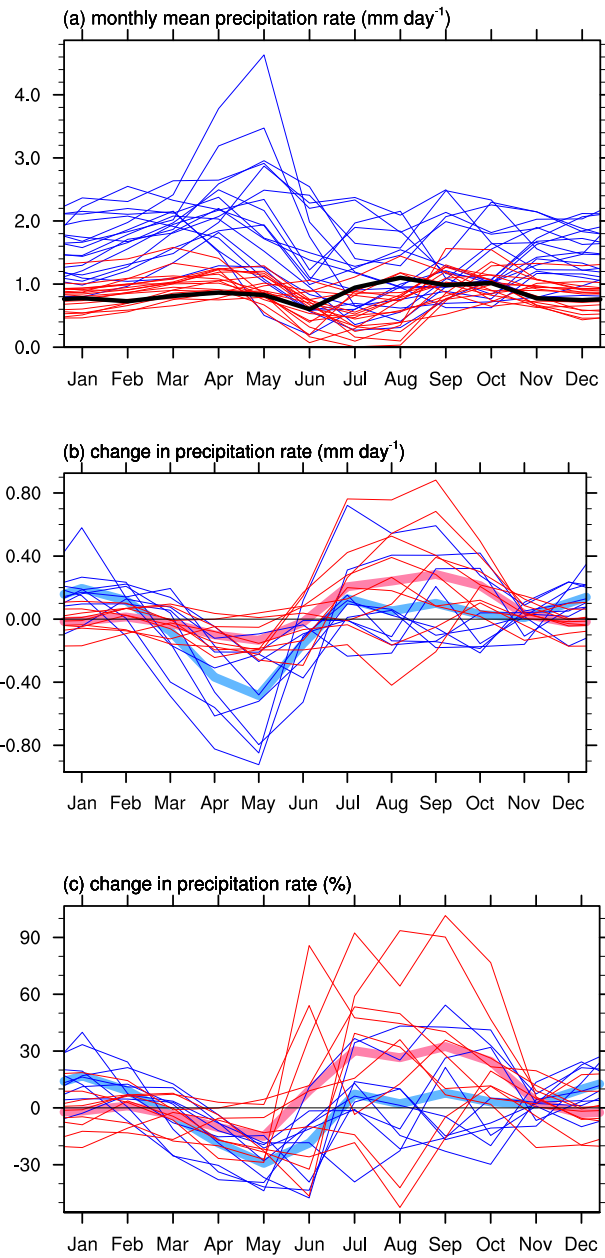


Figure 2. As with Figure 1, only for the Upper Colorado River basin using the predictor fields Q700-T700-V700. Ensemble mean ACSS is 0.56 for EDMs and -0.11 for GCMs.

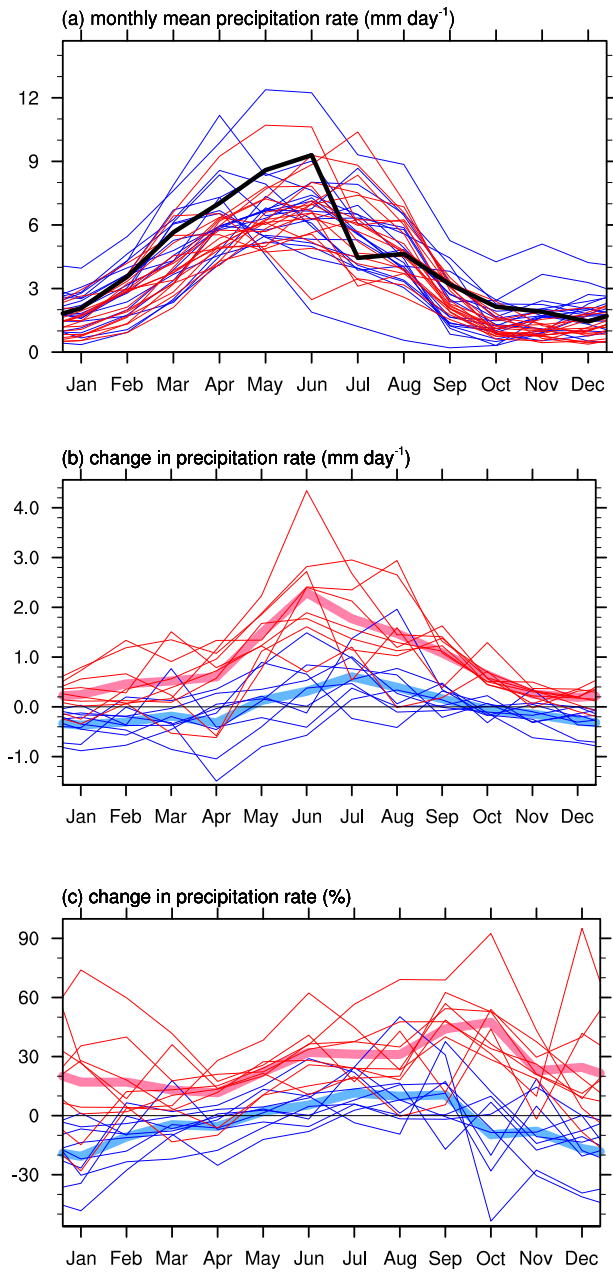


Figure 3. As with Figure 1, only for Jiangxi Province using the predictor fields Q850-U300-U850. Ensemble mean ACSS is 0.61 for EDMs and 0.66 for GCMs.

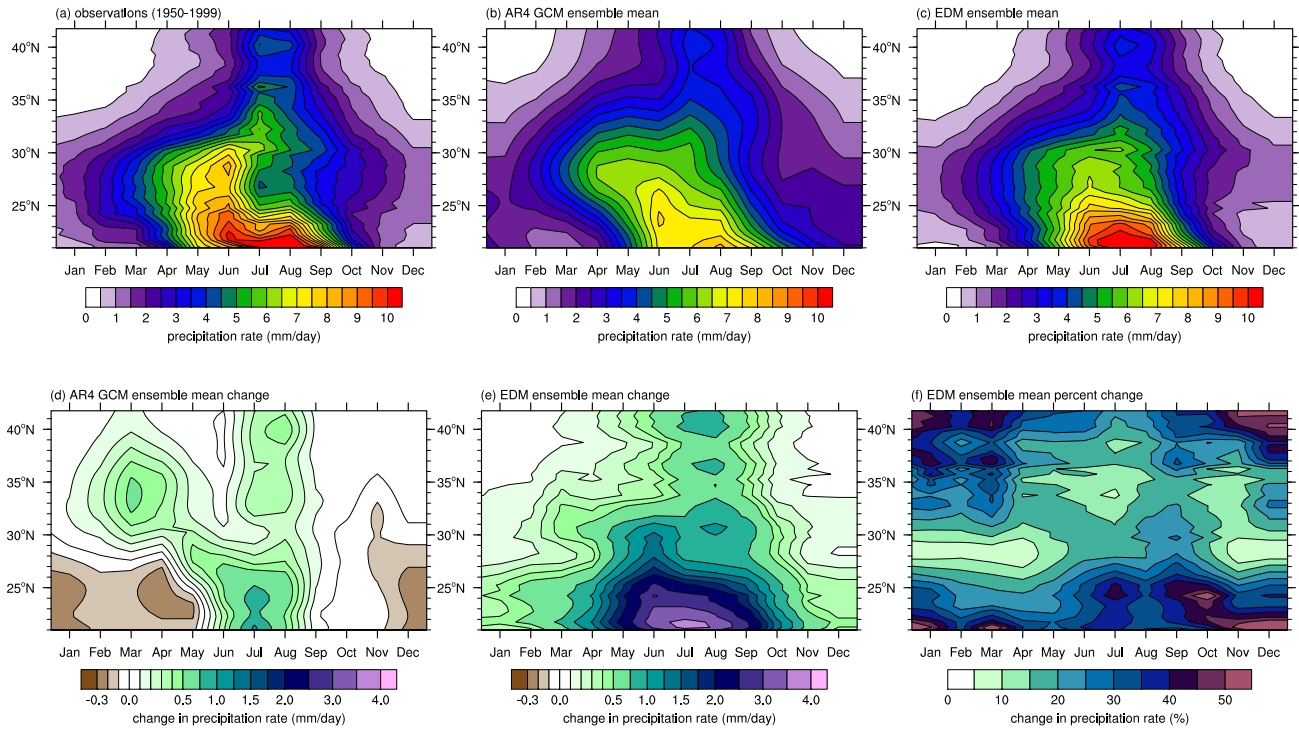


Figure 4. Annual cycle of zonally-averaged (110° - 120° E) precipitation for the East Asian Monsoon region from (a) observations, (b) the 9 most-skillful GCMs, and (c) the 9 most-skillful EDM hindcasts for the period 1950-1999. Projected 1950-1999 to 2050-2099 changes in monsoon precipitation are shown for (d) GCMs and (e) EDM hindcasts in mm/day, and for (f) EDM hindcasts as a percentage of the observed monthly mean.

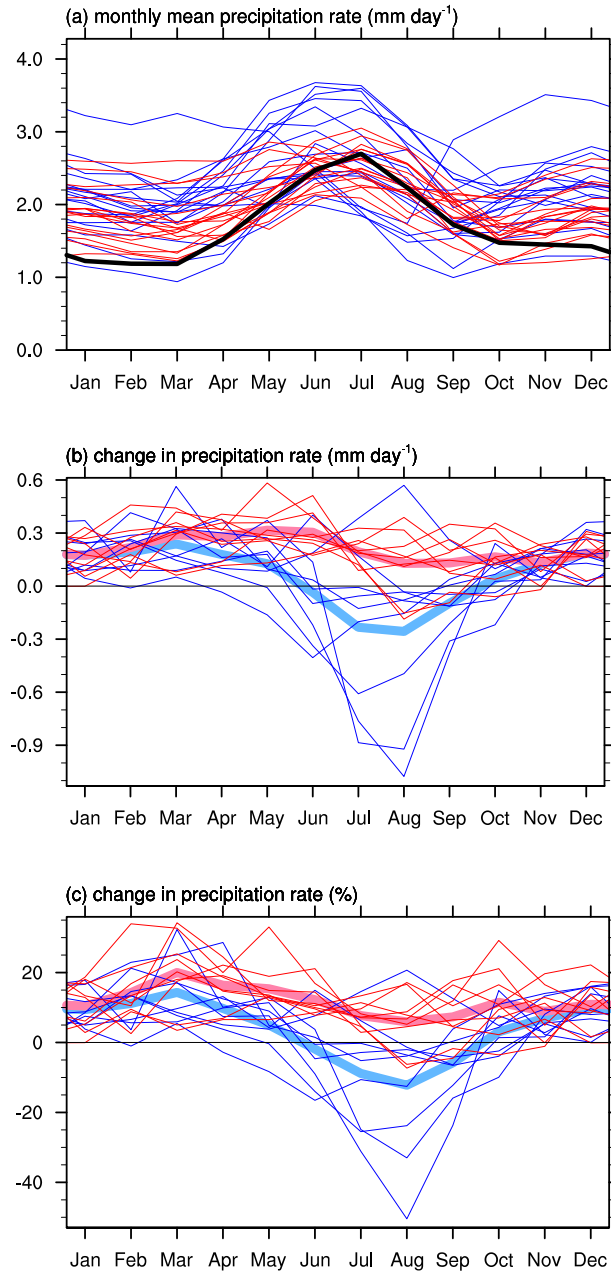


Figure 5. As with Figure 1, only for Central Europe using the predictor fields Q850-Z850. Ensemble mean ACSS is 0.52 for EDMs and 0.37 for GCMs.

Table 1. Predictor variable sets, predictor domain, and test domain for each of the four downscaling regions. Predictor variables are defined as follows: Q850 and Q700 represent specific humidity at 850 and 700 mb; U850 and U300 represent zonal winds at 850 and 300 mb; V850 and V700 represent meridional winds at 850 and 700 mb; and Z850 is the geopotential height at 850 mb.

region	predictor variable	predictor domain	test domain
Southeast US	Q850-U850-V850	73.75°-96.25°W 23.75°-41.25°N	83.0°-92.0°W 31.5°-36.5°N
Upper Colorado River Basin	Q700-T700-V700	103.75°-116.25°W 31.25°-43.75°N	107.0°-111.0°W 37.0°-41.0°N
Jiangxi Province China	Q850-U300-U850	106.25°-123.75°E 11.25°-43.75°N	114.0°-118.0°E 25.0°-30.0°N
Central Europe	Q850-Z850	11.25°W-31.25°E 31.25°-61.25°N	12.0°-19.0°E 48.0°-53.0°N

Table 2. The amplitude of the inter-model spread S in the annual cycle of precipitation from the CMIP3 models (both raw and statistically downscaled) for the period 1950-1999 and 2050-2099 for each of the four regions discussed in this paper. For reference, the observed annual-average precipitation rate over the region is also noted. All entries are reported in mm/day.

region	1950-1999 observed	1950-1999 spread		spread in 1950-1999 to 2050-2099 change	
		raw GCM	downscaled GCM	raw GCM	downscaled GCM
Southeast US	3.67	0.62	0.48	0.37	0.22
Upper Colorado River Basin	0.85	0.46	0.23	0.21	0.12
Jiangxi Province China	4.50	1.09	0.89	0.39	0.38
Central Europe	1.72	0.38	0.30	0.18	0.11